J Polym Res (2014) 21:514
DOI 10.1007/s10965-014-0514-4

ORIGINAL PAPER

New polyimide-based porous crosslinked beads by suspension polymerization: physical and chemical factors affecting their morphology

C. Hulubei · C. D. Vlad · I. Stoica · D. Popovici · G. Lisa · S. L. Nica · A. I. Barzic

Received: 6 January 2014 / Accepted: 16 June 2014 / Published online: 21 August 2014

Abstract Synthesis of a new partial-alicyclic copolyimide based on bicyclo [2.2.2] oct-7-ene-2,3,5,6-tetracarboxylic dianhydride (BOCA) is presented. This polymer was used to obtain porous microspheres by suspension polymerization method. It is copolymerized with N, N'- 4, 4′-diphenylmethanebismaleimide in the presence of two pairs of porogens: 1-methyl-2-pyrrolidone/benzyl alcohol, and 1,4 Dioxane/benzyl alcohol. Influence of different factors, such as diluents composition or crosslinker concentration, on the resulting polymer beads morphology is studied. Various characteristcis including the specific and apparent densities, porosity, pore volume, surface area and mean pore diameter are analyzed. Thermal behavior and tendency to swell in different organic diluents for some chosen samples are also determined. The best polymer beads, obtained in a reaction system with a solubility parameter value of 23.45 MPa $^{1/2}$ and a crosslinker concentration of 40 %, are thermally stable above 400ºC, having a pore volume of 1.28 mL/g, a surface area of 74.20 m2/g and enhanced swelling properties.

Keywords Polyimides · Alicyclic · Suspension polymerization · Crosslinked porous beads

Paper dedicated to the 65th anniversary of "Petru Poni" Institute of Macromolecular Chemistry of Romanian Academy, Iasi, Romania.

C. Hulubei (✉) · C. D. Vlad · I. Stoica · D. Popovici · S. L. Nica · A. I. Barzic
"Petru Poni" Institute of Macromolecular Chemistry, 41A Grigore Ghica Voda Alley, Iasi 700487, Romania
e-mail: hulubei@icmpp.ro

G. Lisa
"Gheorghe Asachi" Faculty of Chemical Engineering and Environmental Protection, Technical University, 73 Dimitrie Mangeron Bdv., Iasi 700050, Romania

Introduction

Nowadays, the development of new polymeric materials with improved properties still represents a major objective both in synthesis and in the quest of new applications.

The porous crosslinked polymer particles [1, 2], especially the ones that are spherical in shape, classified as macro- meso- and microporous, depending on the pore size (>50 nm, 50÷2 nm and <2 nm, respectively) have received great attention because of their various applications including catalytic reaction engineering, separation processes, consumer products (i.e., water softeners and defuming agents), biomedical devices, coating additives or controlled release reservoirs [3–5]. Techniques for the preparation of macroporous polymers were developed almost 40 years ago [6]. From these, suspension polymerization method [7,8] has generally been used in polymer industry for the preparation of robust macroporous (co) polymer networks in beads form (in the micron-size range: 5÷1,000 μm), particularly used as chromatographic separation media, precursors for ion exchange resins, supports for enzyme immobilization and other technological applications [1,9–11].

Crosslinked polymer beads, obtained by radical polymerization reaction of multifunctional monomers or polymers containing polymerizable groups, are very interesting complex structures as a consequence of the kinetic reaction mechanism and the spatial correlation between the resulting polymeric chains [12]. The final (co) polymers properties can be changed by changing the composition of the reacting mixtures, so that the monomers structure and their reactivity become key-factors in the morphologies optimization for specific applications. The most studied monomers used in the polymeric microspheres synthesis are those nonpolar like styrene (ST) and divinylbenzene (DVB) or medium polar such as methyl methacrylate compounds with reactive groups (MMA) [13] the monomers number with functional surface groups being however limited [14].

It is noteworthy that, the use of a reactive polymer as co-reactant in the crosslinked porous beads synthesis provides insight of inducing to the copolymeric product of some from the basic features of the initial structure and, implicitly, some of its properties. From this perspective, of the available synthetic polymers, polyimides (PIs) form a very interesting group. PIs possess good combined properties, including high thermal and chemical stability, high radiation resistance, high mechanical and insulating properties, and, in particular, inherent high refractive index [15]. Due to their features, PIs have been increasingly used as matrix polymers for advanced applications such as in aerospace, microelectronics [16–19], optoelectronics [20, 21], adhesives, gas separation membranes [22], etc.

The use of a PI as base polymer for spherical particulate synthesis correlated with the chemical modification potential of a polyimidic chain by treatment with amine solutions [23], could allow obtaining of micro-particles as carrier matrices with a complex properties profile. Moreover, nitrogen and oxygen atoms included in the molecule structure, give polarity to PIs, these polymers being more polar than those commonly used, St/DVB.

However, mainly due to their strong intra- and intermolecular charge-transfer (CT) interactions [22] there are some limitations especially concerning the PIs processability. In order to decrease CT interactions, different strategies [21], of which the copolymerization [24] or the replacement of aromatic with aliphatic structures [17, 25–28], could be mentioned as relevant. This explains why the PIs containing unconjugated alicyclic units in the main chain, highly soluble, thermally stable, transparent, and almost colorless, are an attractive alternative to some limitations of the aromatic ones [17, 29, 30]..

Only few publications were devoted to the investigation of PIs in spherical particulate shape (exclusively based on monomers) by applying the principles of suspension polymerization technique, [4, 31, 32]. The use of a polyimide to obtain crosslinked porous beads is not mentioned in the scientific literature [33, 34].

The approach proposed in this study consists in the preparation of crosslinked microspheres starting from a polymer chain. The choice relied on the chemistry of a new polyimide having reactive potential due to its C=C double bonds from the main chain [35, 25]. Thus, porous beads were obtained by suspension copolymerization of this new polymer based on the alicyclic BOCA dianhydride with N, N'-4,4′-diphenylmethanebismaleimide (BMI) in the presence of two pairs of pore-forming diluents: 1-methyl-2-pyrrolidone/benzyl alcohol, and 1,4 Dioxane/benzyl alcohol. Influence of several factors, from which, the agitation speed, the stabilization system, the type of porogen, the crosslinker concentration, the initiator and the polymerization temperature, affecting the properties and the morphology of the resulting polymer particles were studied. The synthesis conditions impact on different morphological features was also discussed. It is expected that the findings will have potential for developing polyimidic porous beads materials with improved structures. This will be also useful for future studies relating to the chemical modification of the microparticles surface areas (inner and outer surfaces), so that a large number of imide groups to be activated and to become binding sites for different functional molecules.

Experimental

Reagents and materials

Chemicals from various commercial sources: bicyclo [2.2.2] oct-7-ene-2,3,5,6-tetracarboxylic dianhydride (BOCA), 2,2′-bis-(3,4-dicarboxyphenyl) hexafluoropropane dianhydride (6FDA), maleic anhydride (MA), 4,4′-oxydianiline (ODA), *trans*-1,4-diaminocyclohexane (CHDA), poly (vinyl alcohol): 99 % PVA grade (M_w 14,650); 88 % PVA grade (M_w 50,000, M_w 88,000), benzoyl peroxide (BOP), calcium chloride ($CaCl_2$), 1-methyl-2-pyrrolidone anhydrous (NMP), N,N-dimethylacetamide (DMAc), N,N-dimethylformamide (DMF), dimethyl sulfoxide (DMSO), 1,4 Dioxane (Dx), acetic anhydride, benzyl alcohol (BzOH) and methanol (MeOH) were used as received.

4,4′-Diaminodiphenylmethane (DDM) was recrystallized from ethanol solution and acetone was distilled before use.

Copolyimide synthesis

A new random copolyimide (CPI) have been synthesized by solution copolycondensation reaction of two dianhydrides, BOCA and 6FDA, with two diamines, ODA and CHDA, in NMP as solvent, according to a method previously described for the preparation of other PIs [36]. The reaction proceeded under nitrogen atmosphere, in two steps: synthesis of the poly (amic acid) precursor (PAA) by stirring the comonomers solutions (equimolar ratio between the amine and anhydride groups) for 24 h at room temperature, and thermal imidization for 6 h at 185ºC, to eliminate under nitrogen flow, the resulting water vapors and to obtain the polyimide structure. The reaction mixture was then precipitated in water and the resulting solid polymer was filtered, washed with water and methanol, and dried for 8 h at 105ºC (Scheme 1).

N, N'-4,4′-diphenylmethanebismaleimide synthesis (BMI)

N,N'-4,4′-diphenylmethanebismaleimide was synthesized by Searle reaction between maleic anhydride and 4,4′-diaminodiphenylmethane, in dried acetone, at ambient temperature, followed by chemical cyclodehydration, according

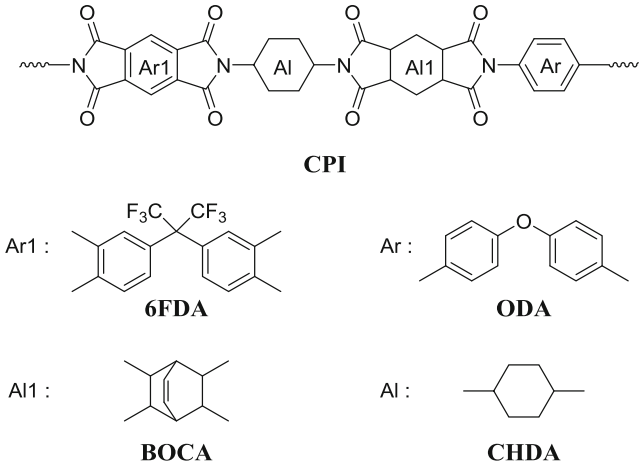

Scheme 1 Copolyimide (*CPI*) and monomer chemical structures

to the literature [37]: m.p. 154–156 °C. Yield: 85.7 %. Elemental analysis (%): Calculated for $C_{21}H_{14}N_2O_4$ (358.34), N (%) calcd./found: 7.82/7.73; IR spectrum (KBr disc): 3,100 (HC=), 2,950 (−CH_2-), 1,770, 1,720 (imide ring, symmetrical and asymmetrical C=O stretching), 1,600, 1,505 (aromatic ring- stretching vibration), 1,380 (C-N stretching), 1,160 (C-N-C bending links), 830 (*p*-disubstituted aromatic ring); ^{1}H-NMR (DMSO-d_6): δ=7.26-7.83 (aromatic ring), 7.14 (vinyl group), 4.12 (−CH_2-).

Porous crosslinked (co) polyimide synthesis

Polymer beads were synthesized by free-radical crosslinking (co) polymerization between CPI and BMI, using suspension polymerization technique. The reaction was carried out in a 250 ml cylindrical three-neck glass reactor, equipped with a mechanical stirrer and condenser. Before the polymerization, the aqueous and organic phases were prepared separately. The aqueous phase was obtained by dissolving the suspension agents (PVA and $CaCl_2$) in distilled water. The organic phase was prepared in inert atmosphere, by mixing the crosslinkable compounds (CPI and BMI), the initiator (BOP) and pore-forming diluents (BzOH and NMP or Dx). The organic phase was added into the aqueous phase after dissolution, at 50ºC, producing a suspension which was maintained stable, under continued mechanical stirring 5 h at 80ºC and 20 h at 90ºC. The resulting polymer beads, washed with boiling distilled water and extracted in a Soxhlet apparatus with acetone and methanol, were finally dried in vacuum.

A general polymerization procedure was as follows: PVA (1.5 g) and $CaCl_2$ (12 g) were dissolved in 100 ml. distilled water. This suspending medium was heated to 80ºC. Meanwhile, a homogeneous solution containing the crosslinkable components CPI (0.5 g), BMI (0.5 g) and porogens, BzOH (6 ml)/NMP (4 ml) was prepared under stirring and at 55ºC, BOP (0.05 g) was added. The solution was immediately poured into the suspending medium and the polymeric beads precipitated in 5 min. The reaction occurred 20 h at 90ºC. The resulting beads were washed with hot water, centrifuged at 2,000 rpm, extracted with acetone and methanol and dried in vacuum at 20ºC

Characterization

Infrared spectra were recorded with a Bruker Vertex 70 spectrometer in transmission mode, at 24 cm^{-1} resolution, by using precipitated polymers ground in potassium bromide pellets. Polymer solubility was determined at room temperature at a concentration of 1 % (w/v).

Weight-average molecular weights (Mw) and number-average molecular weights (Mn) were determined by gel permeation chromatography (GPC) using a Waters GPC apparatus, provided with Refraction and Photodiode array Detectors and Phenomenex-Phenogel MXN column. Polymer solutions of 0.2 % concentration, DMF as eluent and polystyrene standards of known molecular weight for calibration were used for measurements.

Thermogravimetric analysis (TGA) was performed in nitrogen atmosphere at a heating rate of 10 °C/min from 25 to 700 °C with a Mettler Toledo model TGA/SDTA 851. The initial mass of the samples was 2–5 mg. The activation energy of the pre-exponential factor and the reaction order were determined using the Freeman-Carroll differential method [38], which is based on the following equation:

$$\frac{d\alpha}{dt} = A \cdot e^{-\frac{E_a}{RT}}(1-\alpha)^n \quad (1)$$

where dα/dt – variation of the transformation degree in time, A – pre-exponential factor, E_a – activation energy, R – universal gas constant, T – sample temperature in K, α – transformation degree and n – reaction order.

DSC analysis was performed using a Mettler Toledo DSC 1 (Mettler Toledo, Switzerland) operating with version 9.1 of Stare software. The samples were encapsulated in aluminum pans having pierced lids to allow escape of volatiles. A heating rate of 10 °C min^{-1} and nitrogen purge at 120 mL min^{-1} was employed. In order to observe phase transitions the samples were subjected to a heating-cooling-heating cycle in the range of 25 ÷ 350 °C.

The porous networks (vacuum dried for 48 h at 50 °C) were characterized as follows:

The skeletal (ρ) *and the apparent* (ρ_{ap}) *densities* of the polymer beads were measured by the picnometric method with n-heptane (for skeletal densities) and with mercury as the confining fluids (for the apparent densities), when, the beads were out-gassed in a picnometer and then were filled under vacuum with mercury, at 20 °C [10].

The specific surface area S_{BET} was determined by nitrogen adsorption on a Ströhlein Area Meter apparatus, following the BET method [39].

The pore volume values (*PV*) were calculated using the equation:

$$PV = 1/\rho_{ap} - 1/\rho \quad (2)$$

where ρ_{ap} is the apparent density (g/mL) and ρ is the skeletal density (g/mL).

The porosity (%*P*), so-called void volume, (the percentage of pores contained by the beads) was calculated according to the equation:

$$\%P = 100\left(1 - \rho_{ap}/\rho\right) \quad (3)$$

The average pore diameter was calculated according to the relationship:

$$\overline{D} = \frac{4VP}{S_{BET}} \cdot 10^3 \quad (4)$$

The equilibrium weight swelling ratio of the porous copolymers was measured by the centrifugation technique, the excess of the swelling agent being centrifuged from the beads. The swelling degrees were determined by equilibrium swelling in water and methanol. *The swellability coefficient* (*B*) was given by equation [40]:

$$B = \frac{V_s - V_d}{V_d} \cdot 100\% \quad (5)$$

where V_s and V_d are the volume of the swollen and unswollen copolymer, respectively.

The weight of sorbed solvent (*W*) was estimated by relation [41]:

$$W = (W_s - W_d)/W_d \quad (6)$$

where W_s and W_d are the weight of the swollen and unswollen copolymer, respectively.

Atomic force microscopy (*AFM*) was performed by using a Scanning Probe Microscope (Solver PRO-M, NTMDT, Russia) with commercially available NSG10 cantilever. The manufacturer's value for the probe tip radius was 10 nm and the theoretical spring constant was 11.8 N/m. The resonant frequency for this setup was 223 kHz. On the top of each microbead (mounted on a SU001 substrate with a double sided adhesive tape) areas of 10x10 μm^2, 5x5 μm^2 and 2x2 μm^2 were evaluated in tapping mode, all the images being collected in air, at room temperature (23ºC). For image acquisition and analysis Nova v.1.26.0.1443 for Solver software was used.

To evaluate the topography, surface parameters such as *surface skewness* (S_{sk}), *coefficient of kurtosis* (S_{ku}) and *roughness parameter* or rugosity (f_r) were used. Considering that the information obtained on surface topography by AFM technique is stored and processed in digital form as a matrix Z (N, M), where N is the number of points along of scan lines and M is the number of lines, the *surface skewness* is defined as

$$S_{sk} = \frac{1}{MN\ S_q^3} \sum_{k=0}^{M-1} \sum_{l=0}^{N-1} [z(x_k, y_l)]^3 \quad (7)$$

and *the surface kurtosis* is defined as

$$S_{ku} = \frac{1}{MN\ S_q^4} \sum_{k=0}^{M-1} \sum_{l=0}^{N-1} [z(x_k, y_l)]^4 \quad (8)$$

where: z is the height of each point of coordinates x_k şi y_l [42] and S_q is the root mean square roughness.

The roughness parameter (a measure of small-scale variations or amplitude in the height of a surface) is defined as

$$f_r = \frac{A_r}{A_g} \quad (9)$$

where: A_r is the real (true, actual) surface area and A_g is the geometric surface area [43].

Environmental Scanning Electron Microscope (ESEM) type Quanta 200, coupled with an energy dispersive X-ray system, was used also to investigate polymer beads morphology

Results and discussion

Structural characterization of the copolymers

The linear CPI was synthesized in two steps, by combining aliphatic/aromatic pairs of monomers: the dianhydrides BOCA/6FDA and the diamines CHDA/ODA (Scheme 1).

The new CPI, with a number-average molecular weight, Mn, of 70 000 g/mol, and a thermal stability above 400ºC, is soluble in the test solvents at room temperature including NMP, DMAc, DMF, DMSO, and also in Dx at heating. The good solubility is due to the random structure containing co-planar and non co-planar alicyclic groups, and ether flexible linkages which, by cumulative effect, reduce the symmetry,

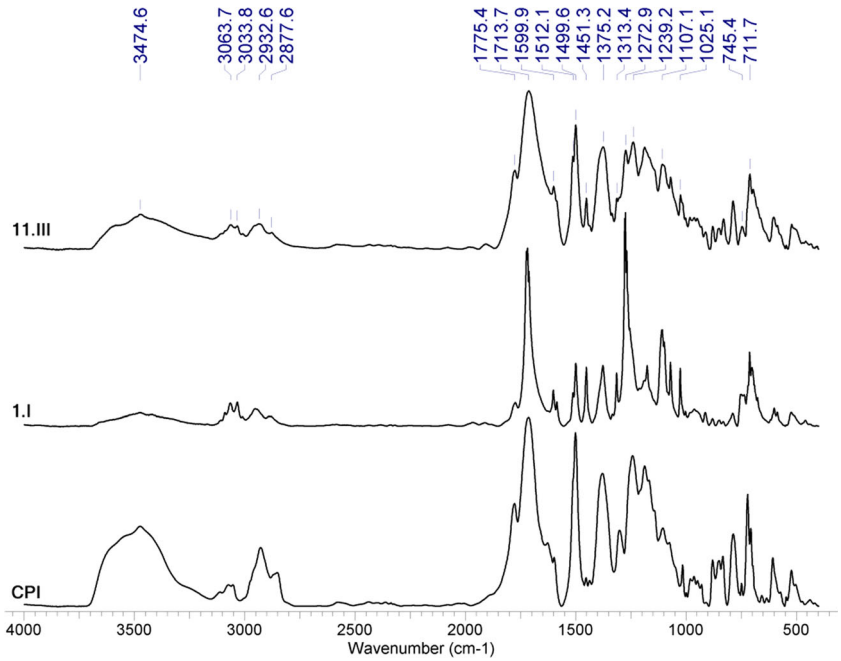

Fig. 1 FT-IR spectra of: **CPI**, **1. I** and **11. III** samples

rigidity and the degree of polymer chain interaction [44], decreasing the close packing.

Bead-shaped crosslinked (*co*) *polymers* using different components ratios CPI/BMI (50/50, 60/40, 65/35, 70/30 and 75/25), the same stabilization conditions and two pairs of porogens were synthesized.

The FTIR spectra for the CPI and two obtained crosslinked samples (Fig. 1) demonstrate the synthesized structures. Distinct peak features of imides appear around 1,777 and 1,713 cm^{-1} (symmetric and asymmetric stretching vibration of C=O linkages in imide ring), 1,378 and 723 cm^{-1} (C–N–C stretching, and imide ring deformation), respectively. The peaks near 1,512 cm^{-1} (=CH) and 3,063–3,033 cm^{-1} (C–H) - from the benzene ring - confirm the aromatic structures. Other absorptions at 2,932 and 2,877 cm^{-1} suggest the presence of CH_2 linkages in the aliphatic units (asymmetric and symmetric CH_2 stretching vibrations). The peak at 711 cm^{-1} is related with the C=C bond from the bicyclic structure [25], while the absorption bands at about 1,239 cm^{-1} and 1,375 cm^{-1} are associated with the ether bridge and hexafluoroisopropylidene groups (6 F) into polymer backbones, respectively.

Factors affecting the suspension polymerization

Effect of agitation speed

It is well recognized that the final particle size and particle size distribution are decisively impacted by the initial drop size distribution of the monomer/water dispersion and the controlled breakage/coalescence processes in the early stages of polymerization [45]. In our experiments, a mechanical agitation was applied throughout the whole process to keep the monomer droplets well dispersed.

The results showed that large particles are formed for agitation speeds between 200÷300 rpm and 900 rpm

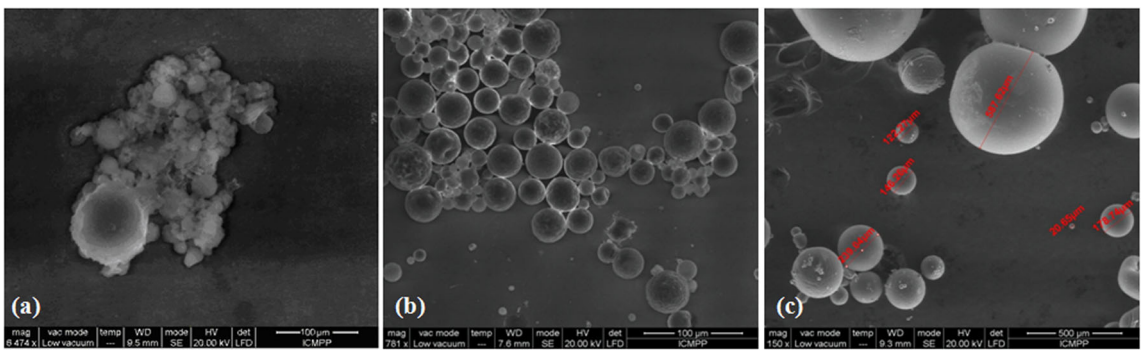

Fig. 2 Effect of the agitation speed on the particle size: **a** 210 rpm, **b** 420 rpm and **c** 900 rpm

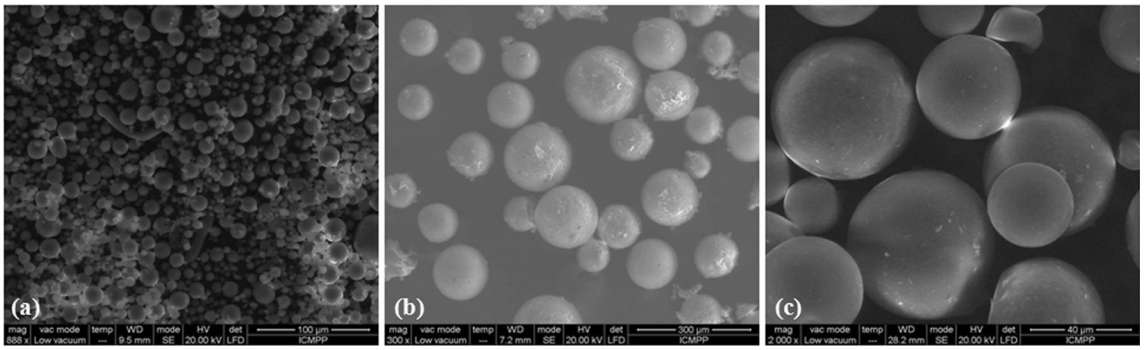

Fig. 3 Effects of the PVA molecular weight and hydrolysis degree on the particle size. PVA: **a** M_w 14,650, 98 % hydrolysis degree, **b** M_w 50,000, 88 % hydrolysis degree and **c** M_w 88,000, 88 % hydrolysis degree. Polymerization system: solubility parameter δ=23.37 $MPa^{1/2}$, crosslinker (BMI) 40 %, stabilization system: (1.5%PAV+12%$CaCl_2$)

respectively, while *at a moderate agitation speed* of about 400 rpm, small particle are obtained. One possible explanation could be that *at a low agitation speed* there is an insufficient splitting of the initial monomer droplets, while a*t a high agitation speed* there is a high probability that many collisions to finish in coalescence, because, the very small initial monomer droplets can be cluttered due to an inadequate stabilization. The results are in agreement with the literature data [46], which report a U-shaped addiction of the mean drop size on the agitation speed, typical for the complex nature of breakage/coalescence processes occurring in suspension systems.

Figure 2 presents such situations where droplet collision and breakup cannot be prevented. It may also observe that, at different agitation speeds, particles of various sizes which are almost always polydisperse were obtained. It is to be noted that coalescence decreases up to a completely elimination when the concentration of the bulk stabilizer increases to the so called critical surface coverage [47].

Effect of the suspension stabilizer

The morphology of the resulting crosslinked (co) polymers is in a great extent determined by the type of the used suspending agent, since it protects the droplets against collision during polymerization. Throughout the whole process of suspension polymerization, the two phases organic and water, remain separated. The polymerization takes place in the suspended droplets that act like isolated micro reactors. Various polymeric structures, such as partially water-soluble polymers cellulose derivatives and partially hydrolyzed poly (vinyl alcohol) (PVA) are employed as stabilizers.

In our experiments, PVA with a hydrolysis degree of 98 and 88 mol %, respectively, were used. The average degree of polymerization for the 98 % PVA grade was 14,650, while for the 88 % PVA grade was 50,000 and 88,000. The results revealed that PVA with the highest molecular weight and partially hydrolyzed (Mw=88,000, 88 %) is the best suspension agent, whereas PVA with the lowest molecular weight and the highest hydrolysis degree (Mw=14,650, 98 %) leads to unstable systems.

Two issues should be mentioned, namely: the linear copolyimide has a pronounced hydrophobic character due to the non-polar alicyclic sequences and the 6 F bridges from the backbone structure [48], and that PVA, due to its hydrophilic character, adjusts the polymer particles size by its positioning at the surface, outside of the resulting monomer droplets. By varying the hydrolysis degree one can alter the PVA hydrophobicity and by default, its conformation and surface activity

Scheme 2 Schematic representation of some possible reactions in a FRCC

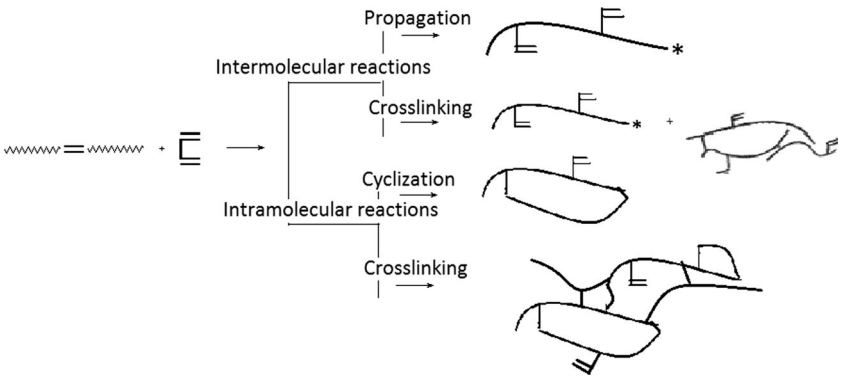

at the monomer/water interface [46]. A high hydrolysis degree increases the hydrophilic phenomenon so that, the PVA molecules do not adsorb strongly enough at monomer–water interface to form a coherent film and inhibit the coalescence of droplets. This explains the decrease of suspension stability and the increasing trend of the mean droplet size. By contrast, the moderately hydrolyzed PVA, with a more active surface at the droplet interface, enhances the system stability, and shifts the drop size to smaller values possibly due to a changed interfacial tension which affects the droplet breakage/coalescence rates (Fig. 3). As a conclusion, even if the PVA species with low molecular weight are more active surface agents (being prone to a stronger action than the higher molecular weight ones) the hydrolysis degree seems to be the key factor for the adsorption balance of PVA at the monomer–water interface and, implicitly, for the stabilization of the discussed systems.

The experiments showed that for an aqueous/organic phase ratio of 10/1 and an amount of poor solvent in the diluent mixture between 40÷50 wt.% regular spherical beads were obtained. A proportion of poor solvent outside this range resulted in agglomerated particles. Agglomerates were also formed at very low concentration of $CaCl_2$ (4 wt.%) in aqueous phase, while above this value a gradual decreasing in particle size was noticed. Minimum size values for a concentration of 12 wt.% were observed.

Effect of the initiator and the temperature

When polyunsaturated compounds are incorporated into a growing chain, some double bonds react and some become pendant. These pendant double bonds take part in the copolymerization and are gradually crosslinked. A schematically representation for possible reactions of the chain-end macroradicals which occur in a free-radical crosslinking (co) polymerization (FRCC), is presented in Scheme 2.

Considering the polyunsaturated nature of CPI and the steric accessibility of the double bonds into the macromolecular chain as compared with small molecules, a larger amount of benzoyl peroxide (BOP) was used comparatively with conventional free radical polymerization. This allowed better performances providing more reaction centers and by default, an increased polymerization rate [49].

All the reactions occurred in isothermal regime at 90ºC for 20 h. *The temperature* value was selected to assure a high decomposition rate of the initiator (resulting greater number of free radicals and implicitly more nuclei and microspheres [50]) and also, a high solvating power of the diluents. Both influences contributed to shift the pore size towards smaller pores, due to the increase of the polymerization rate with temperature [2, 50]. Table 1 presents some results concerning the effects induced by the stabilization system and the initiator concentration on the particles yield and size. One can notice that the yield enhances with increasing of the BOP feed amount in the reaction mixture, while the bead size decreases with increasing of the molecular weight of the PVA stabilizer.

Table 1 Effects of stabilizer and initiator on the yield and particle size of the crosslinked beads

Factor	Stabilizer[a)]			Initiator [b)]				
Quality	$M_{w\ PAV}$ 14,650	50,000	88,000	BOP				
Quantity (%)	1.5 % PAV+12 % $Ca\ Cl_2$			1.4	2	3	4	5
Yield (%)	66	73	78	52	57	64	69	73
*Particle size, μm	5–60	35–500	20–200	30–700				

[a)] Polymerization system: crosslinker (BMI) 30 %, initiator (BOP) 5 %; [b)] Polymerization system: crosslinker (BMI) 30 %, stabilization system (1.5%PAV+12%$CaCl_2$); PAV: M_w 50,000, 88 % hydrolysis degree

Factors affecting the resulting polymer beads morphology

Effect of diluents and crosslinker

Porous structures start to form when the amount of diluent and crosslinker pass a critical value. The resulting polymers morphology (studied on samples with mechanical strength, washed and dried), was investigated as a function of the pore-forming diluent quality (BzOH/NMP and BzOH/Dx) and the crosslinking components molar ratio in the reaction mixture (CPI/BMI: 50/50, 60/40, 65/35, 70/30 and 75/25, respectively). The ratio between diluent (D) and monomers (M) was constantly equal to 10:1 (ml/g). All the other parameters were kept unchanged.

In suspension polymerization pores are formed in the presence of a suitable porogen (usually called diluent, inert medium, etc.), which causes phase separation during the polymerization process [1]. The quality of the solvent used as porogen depends on the thermodynamic quality (affinity), expressed as the relationship between the solvent and solute (*solubility parameter*). The co-reactants quantity and the polymer-solvent interaction in the reaction mixture, determine the porous network structure. The structure formation can be explained in terms of differences between the solvent and polymer interaction parameters. The Hildebrand solubility

Table 2 Solubility parameter values for the used components

Components	δ ($MPa^{1/2}$)*
Benzyl alcohol	23.8
NMP	22.9
1.4 Dioxane	20.5
CPI	24.04
BMI	24.48
polyBMI	25.19
crosslinked	24.56

*The δ values of porogene selected from literature [53]

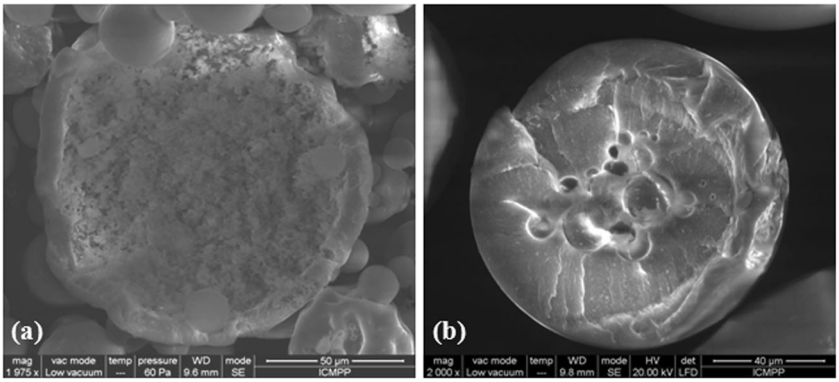

Fig. 4 Scanning electron micrographs of fractured beads samples containing 50 % BMI: **a** in BzOH/NMP: 60/40; **b** in BzOH/Dx: 60/40

parameter theory proved in many cases, extremely useful in predicting the physical characteristics of the crosslinked polymers [51]. Table 2 presents the solubility parameters (δ) values for the diluents and the reaction components [52]. Consistent with this theory, BzOH can act as *good solvent* due to its almost similar thermodynamic properties as the crosslinked compounds, in contrast with the other two solvents, NMP and Dx, which behave as *poor solvents*.

The results revealed that only the mixtures of those diluents containing BzOH ensure the porous polymeric beads formation with mechanical strength. Both, NMP and Dx respectively, used alone as pore-forming diluents, resulted in very incoherent pore structures caused by a much too earlier phase separation, while BzOH, used alone as porogen, led to porous networks without resistance (possible due to a large interconnected pores number).

Figure 4 presents SEM images as detail for the internal structure of two fractured samples with the same chemical composition, but synthesized using different porogen systems. It is noticed the porogen effect of a thermo-dynamically good solvent which allows to obtain fine-meshed network structures, with high surface area and small pore size (Fig. 4a). This is because the polymer remains fully solvated up to a high degree of conversion in the reaction system. In opposition, Fig. 4 b presents a more coarsely porous structure, with a small surface area and a large pore volume, which is in fact, the porogen effect of a poor solvent, reflecting the incompatibility between its molecules and the resulting polymer network segments [2, 54].

In order to investigate the influence of the δ-parameter value variation on the resulting polymers morphology, three series of porous polymers, by using two couples of diluents were synthesized. Matrices with different morphological characteristics, by changing the quality and the components ratio in the mixed solvents were obtained (Table 3).

The solubility parameter for the diluents mixture used as porogen, $\delta_{mix,}$ was calculated as follows [55]:

$$\delta_{mix} = \frac{X_1 V_1 \delta_1 + X_2 V_2 \delta_2}{X_1 V_1 + X_2 V_2} \tag{10}$$

where: X_1, V_1 and δ_1 are volume fraction, molar volume and the solubility parameter of the first diluent, and X_2, V_2 and δ_2 are volume fraction, molar volume and the solubility parameter of the second porogen medium.

The resulting crosslinked (co) polymers exhibit different morphologies depending on the used diluent (implicitly its solvating power) and the crosslinker content in the reaction mixture. Taking into account the δ-parameter as basic factor in the porous morphology formation, and plotting the experimental results for different crosslinking degrees, a strong dependence between these two synthesis parameters and the morphological polymer characteristics can be observed.

According to *the solubility parameter* value deterioration (i.e. the variation of the quality and/or the quantity of the diluents inside the mixture, series **I-III**) the average pore size

Table 3 Recipe used in reaction systems to prepare the samples

Sample's code	Series	BMI (%)					BzOH (X_1)	NMP (X_2)	Dx.(X_2)	$^{*}\delta_{mix.}$ ($MPa^{1/2}$)
		5	30	35	40	50				
	I	1	2	3	4	5	0.6	0.4	-	23.45
	II	6	7	8	9	10	0.5	0.5	-	23.37
	III	11	12	13	14	15	0.6	-	0.4	22.64

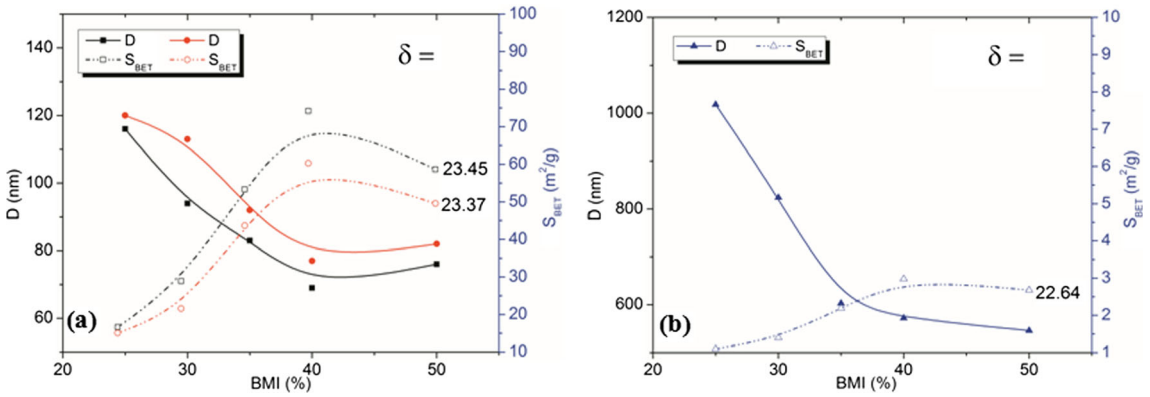

Fig. 5 The influence of the crosslinker concentration on the mean pore diameter in systems with different solubility parameters values: **a** series I & II; **b** series III

changes from small pores to large pores as show the curves shape from Fig. 5 a, b.

Macroporous (co) polymers with relative small pores, whose average size lies within the range of 0.069 ÷ 0.120 μm were obtained when a BzOH/NMP mixture was used as inert medium (series **I**, **II**). The outstanding differences referring to the morphological characteristics of the beads from series **III** vs. **I** and **II** could be associated with the qualitative influence of the poor solvent on the solvation power of the diluents mixture (Dx being less polar comparatively with NMP). For a higher content of NMP in the diluents-mixture (series **II**) at the same BMI concentration, a minimal variation of the pore size is obtained, while when Dx is used instead of NMP (series **III**) significant changes appear (Fig. 5b). Also, the specific surface area variation at the same crosslinking degree shows maximum values for the (co) polymers from series **I**, the system exhibiting the best solubility parameter value.

At various *crosslinker concentrations* and the same degree of the monomer dilution and diluent quality, the experimental data showed that the pore volume and the specific surface area increase with raising the BMI amount to a certain threshold, of about 40 % (after these this characteristics decrease). The apparent density decreases simultaneously up to the same BMI concentration (Fig. 6). The results are consistent with the literature data [1] which confirm such a threshold related to the solvent and crosslinker content in macroporous structures synthesis.

An increased crosslinker amount in the reaction system leads to the creation of more rigid structures, with very crosslinked nuclei and, by default, to an increase of the pores number and a decrease of their size. At the same time, the crosslinker content has a major impact on the specific surface area of the resulting structures [2] the main part of the specific surface area of a polymer bead arising from the surface of these nuclei. The quite different SBET variation for series **III** might be associated with the porogen effect – low solvation power – which determines the earlier phase separation during polymerization and bigger clusters formation.

Microscopic analysis

The changes of the microbeads morphology were evaluated by AFM and SEM methods (Table 4). The AFM images were processed by a plane correction to achieve the best accuracy. For a proper comparison of the surface roughness, the rugosity (roughness parameter) was obtained as the ratio of the true surface area and geometric surface area.

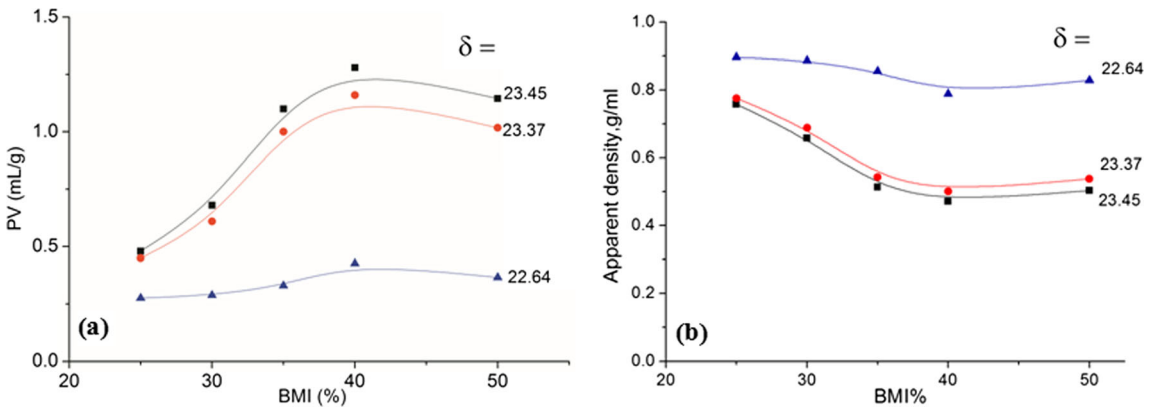

Fig. 6 The influence of the crosslinker concentration on the: **a** pore volume and **b** apparent density in systems with different solubility parameters values

Table 4 Roughness parameters and pore characteristics obtained from AFM investigations for crosslinked microbeads surfaces: **1. I**, **4. I**, **11. III** and **14. III**

Sample	Roughness parameters			Pores characteristics					
	S_{sk}	S_{ku}	f_r	d_{min} (μm)	d_{max} (μm)	A (μm^2)	P (μm)	f_{shape}	f_{elong}
1. I (25%BMI)	−0.03	−0.50	1.36	1.176	1.961	2.48	12.28	0.19	0.56
4.I (40%BMI)	0.19	2.00	1.04	0.06	0.08	0.03	0.19	0.25	0.75
11. III (25%BMI)	−0.34	−0.23	1.35	0.588	1.451	3.28	9.61	0.41	0.55
14. III (40%BMI)	−0.06	0.08	1.03	0.25	0.41	0.05	1.18	0.42	0.61

Figure 7 presents the representative tapping mode height is replaced with: Figs. 7A and 7B present the representative tapping mode height images obtained for some microbeads surfaces, together with their corresponding SEM data. By analyzing the results, porous structure of all these materials is well visible. The roughness calculations, commonly used in materials science to characterize surfaces, indicate that crosslinking degree strongly influences the actual surface area, and therefore the roughness parameter (see BMI concentrations values from Table 3 and f_r from Table 4).

The height histograms of the topographical images, showing the statistical distribution of z-values (heights) within the image, are presented in Figs. 7A and 7B for the samples **1. I**, **4. I**, and for **11. III**, **14. III**, respectively.

Two statistical parameters were used for the height histogram evaluation: the *surface skewness* (S_{sk}) which describes the height distribution asymmetry and *coefficient of kurtosis* (S_{ku}) which measures the spikiness or the randomness of surface heights. The obtained results (Table 4) were discussed according to the principles of the statistical theory [56]. Regarding the S_{sk} *parameter*, it can be seen that, for values of $S_{sk}<0$, surfaces with holes were obtained (samples **1. I**, **11. III** and **14. III**), while for values of $S_{sk}>0$ a flat surface with peaks - explained by the small diameter of the pores and the predominance of other formations - was observed (sample **4. I**). Concerning the S_{ku} *parameter*, the values lower than 3.00 indicate surfaces with bumpy morphology, while the negative values, obtained for the most prominent pores (samples **1. I**, **11. III**) reveal a topography which displays grain clustering.

In Figs. 7A and 7B, the cross-section profiles taken along the solid lines from 2D images highlight the existence of porous formations over the surfaces. These pores have different dimensions and shapes, their appearance being influenced by the porogen characteristics and the crosslinking degree.

Corroborating the data regarding the pores diameters, from Table 4, and the images from Figs. 7A and 7B, it is noteworthy that low concentrations of BMI in reaction system resulted in microbeads formation with larger pores size (samples **1. I**, **11. III**) than those obtained using high crosslinker monomer amounts (samples **4. I**, **14. III**). The calculations of the displayed shape parameters were performed on pores considered representative for the entire investigated surface. The shape factor is defined as

$$f_{shape} = \frac{4\pi A}{1.064\ P^2} \tag{11}$$

where A is the pore area, P is the pore perimeter and the factor 1.064 [56] corrects the perimeter for the effects produced by the image digitization [57]. The elongation factor is expressed by equation

$$f_{elong} = \frac{d_{\min}}{d_{\max}} \tag{12}$$

where d_{min} and d_{max} are the minimum and maximum Feret diameters.

Considering the values of these factors displayed in Table 4 and taking into account that the *shape factor* is 1 for a smooth circumference, it is observed that all the investigated crosslinked microbeads have a shape factor lower than 1 and present porous formations with irregular contour. Also, the *elongation factor*, which depicts the elongation level of the pores, independently of the contour, is lower than 1 for all the samples. This describes an almost circular form of the pores for **4. I** sample surface (f_{elong}=0.75), and an elliptical form of the pores for the other samples, also visible in 3D height images from Figs. 7A and 7B.

AFM analysis confirms crosslinked copolymers formation mechanism, first proposed by Kun and Kunin and developed by Dusek as (1) the production and agglomeration of highly crosslinked gel microspheres, (2) the binding together with agglomerates and the matrix structure fixation. In this context, the bead porosity is the result of the phase separation which occurred during polymerization in the presence of the porogen [58].

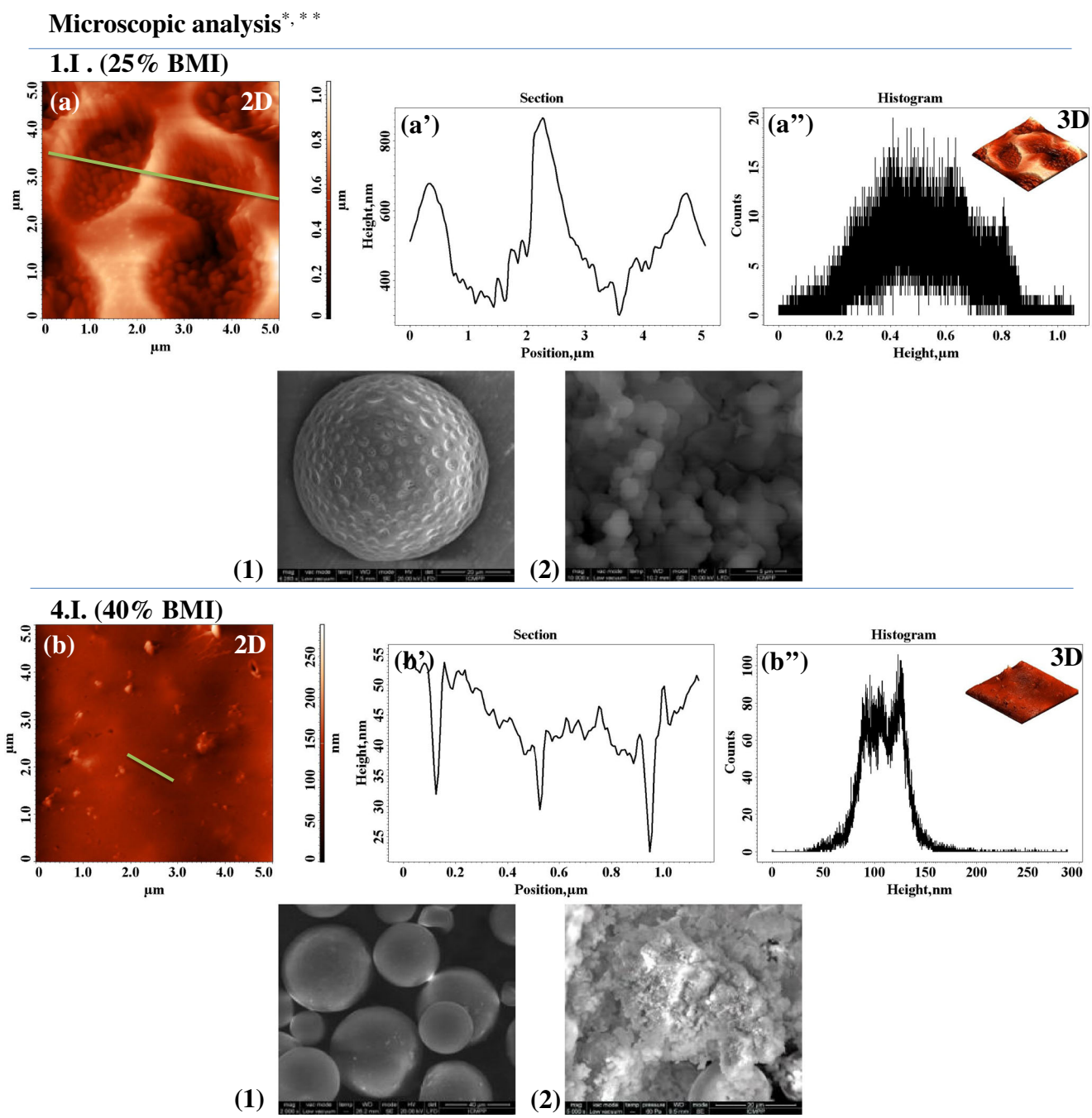

Fig. 7 Microscopic analysis: *2D AFM height images (*a*, *b*), cross-section profile taken along the line from 2D image (*a*', *b*') and height histogram with 3D image (*a*", *b*") as inset of crosslinked microbeads surfaces of samples no. **1. I** and **4. I**; **SEM images: (1) external surface bead; (2) internal structure. Microscopic analysis: *2D AFM height images (c, d), cross-section profile taken along the line from 2D image (c', d') and height histogram with 3D image (c", d") as inset of crosslinked microbeads surfaces of samples no. **11. III**, and **14. III**; **SEM images: (1) external surface bead; (2) internal structure

Characterization in a swollen state

An optimal morphological structure for various application domains has been of great interest, both in industry and science domain. The sorption capacity or swelling in solvents is advantageous for the porous polymers performance as adsorbents. Water adsorption is known when these products tend to swell with solvent, even if the solvent is not one that is normally considered compatible with chemical structure of the crosslinked composition [59].

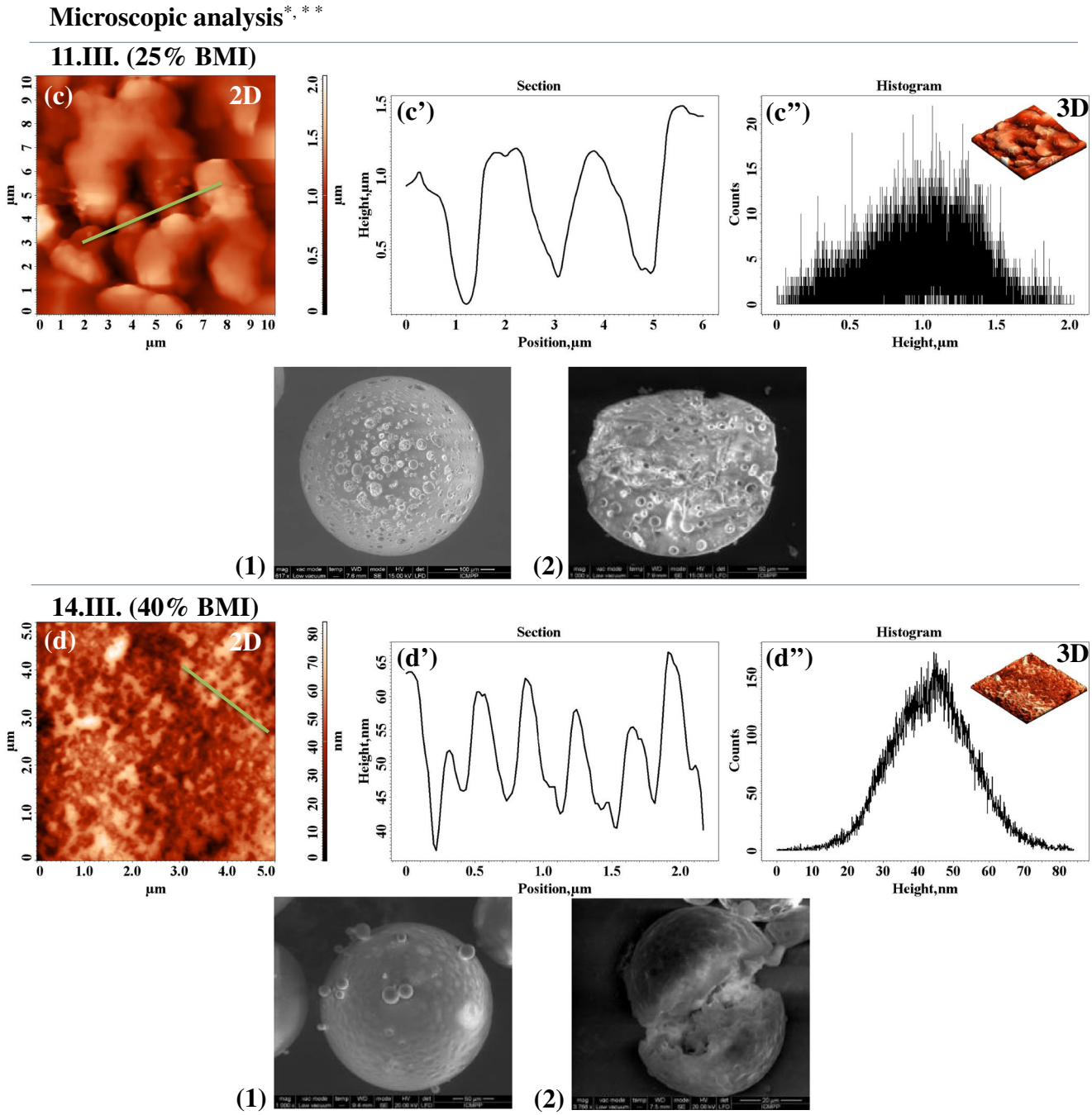

Fig. 7 (continued)

The equilibrium weight swelling ratio, W, (mass of swollen polymer/mass of dry polymer) includes the amount of solvent taken by (1) the swelling of network and (2) the filling processes. An increase of the weight-swelling ratio actually means an increased pores volume which is filled by the solvent.

The volume swelling ratio, B, caused by the crosslinked polymer swelling ("solvation") represents only the solvent amount included in the first process of W data measuring. To estimate the tendency to swell in different solvents, W for the (co) polymers from series **I** was measured. Here it should be noted that the swelling behavior depends on the attractive force between the solvent and the network segments, differences in the structural characteristics of the studied samples playing a decisive role in the obtained results (B and W values). Table 5 presents the swellability coefficients in methanol and water.

All the investigated samples swell significantly in water and methanol. This fact could be considered a cumulative effect of (1) the interactions between the polar solvent and the PI microspheres molecules - imide rings being polar sequences - (2) the crosslinked network porosity - facilitating the solvent access in the entire mass - and not lastly, (3) the polymer chain structure - a random alicyclic/aromatic PI – with its macromolecular conformation, which affect the resulting crosslinked (co) polymers morphology. The experimental results show that swelling data values are improved when increase the crosslinking agent concentration [60], the best results being achieved for sample **4. I**, having the largest values for the surface area and porosity, respectively. This is in connection with the fact that, porous (co) polymers with a high content of crosslinking monomer, prepared in the presence of solvating diluents, have more ordered structures and a light solvation and swelling of the polymer chains [61].

Thermal behavior

The thermal behavior of the synthesized crosslinked CPI/BMI microbeads was studied by means of thermogravimetric analysis (TGA) and differential scanning calorimetry (DSC), in order to reveal the structural changes occurring in heating.

The thermogravimetric curves (TG) and derivative thermogravimetric curves (DTG) - detected by TGA - revealed a complex degradation mechanism both for the crosslinkable components (CPI and BMI) and for the resulting crosslinked beads. The thermal stability of these materials is very good, with decomposition temperatures above 400 °C. Figure 8 displays a comparison between the DTG curves of the CPI, BMI some resulting samples.

One can observe that the main thermal decomposition stage of the PI beads presents a Tpeak (temperature at which the degradation rate reaches its peak) in a temperature range very close to the main thermal decomposition stage of the crosslinking components, involving changes in the mass loss percentage as compared to these, BMI and CPI, respectively (Fig. 9).

Table 5 Crosslinked copolymers swelling data

sample	BMI%	B (%) (in water)	W (g/g)	B (%) (in methanol)	W (g/g)
1.I	25	13	0.11	71	0.52
2.I	30	32	0.26	96	0.70
3.I	35	34	0.28	106	0.77
4.I	40	67	0.48	195	1.03

The kinetic processing of thermogravimetric data for the main stage of thermal decomposition (the range of 403-510 °C) showed that, for the crosslinked bead, the reaction order values vary from 1.7 to 3.0 and the activation energies values are higher than 200 kJ/mol. By comparing the activation energies values in this decomposition stage, the following sequence of the thermal stability for the investigated samples was obtained (Table 6).

CPI < 11.III < BMI < 1.I < 14.III < 4.I.

Differential scanning calorimetry (DSC) studies were conducted in order to determine phase transitions. The DSC curves (two heating and one cooling cycles) read for the initial linear copolyimide, and some crosslinked bead samples, did not exceed the 25÷350ºC temperature range.

Considering that the first heating cycle is influenced by the sample history, Fig. 10 shows a comparison between the curves corresponding to the second heating cycle. The fact that only the linear copolyimide, CPI, exhibits a vitrification temperature (T_g=324 °C), and the activation energy values (of the main thermal decomposition stage) for the investigated polymer beads are higher than of CPI (with 40 kJ/mol) may confirm the occurrence of the crosslinking process.

Conclusions

A new soluble and thermally stable crosslinkable aromatic/alicyclic polyimide based on BOCA dianhydride has been synthesized. Porous crosslinked (co) polymers as bead shape,

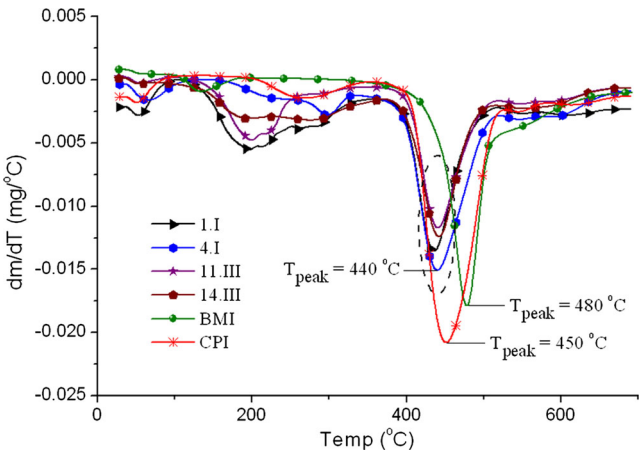

Fig. 8 DTG curves for CPI, BMI and some polymer beads samples

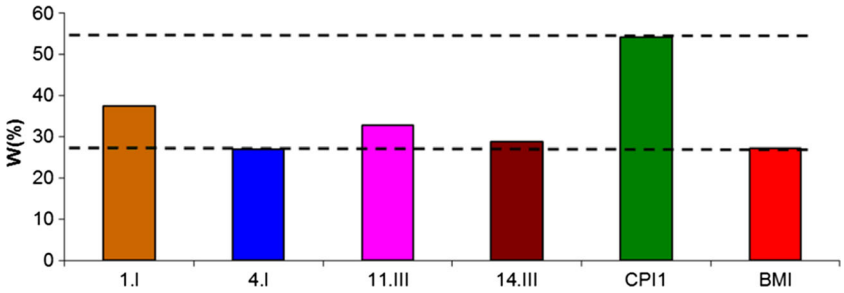

Fig. 9 Mass loss percentages within the 400 and 500 °C range for CPI, BMI and some polymer beads samples

with a good spherical geometry, from this new unsaturated polyimide and a bismaleimide structure, have been obtained by suspension polymerization.

Three series of polymeric samples, using different diluent mixtures (by changing the quality and the ratio between the components) and different BMI concentrations have been prepared. The porogens and crosslinker content essentially control the microbeads morphology. The more closely mutual solubility parameter values (series **I&II**) macroporous crosslinked (co) polymers with smaller pores (average size 69÷1,200 nm) and large surface area (17÷59 m^2/g) are obtained. At the same degree of monomer dilution and diluent quality, the pore volume and total porosity increase with raising the BMI content to a certain threshold of about 40 %, after that, these characteristics decrease.

The AFM investigations confirm crosslinked copolymers formation mechanism and reveal that all the synthesized crosslinked microbeads are porous formations with irregular contour. An almost circular form of the pores for **4. I** sample (f_{elong}=0.75) and an elliptical form of the pores for the others was observed. SEM images confirm the (co) polymers from series **I** as exhibiting more homogeneous morphologies, with smaller pores, comparatively with those obtained in the other two series.

All samples significantly swell in water and methanol, due to the interactions between the polar solvent and the imide rings from the crosslinked beads structure, the swellability coefficient (B) and the weight of sorbed solvent (W) being closely related to the structural characteristics of studied (co) polymers. The swelling values increase with the augmenting the crosslinker (BMI) content.

The polyimidic support based on CPI/BMI (co) polymer induces a high chemical and thermal stability ensuring to the resulting structures an appropriate reinforcement and rigidity, in order to maintain the network porosity and avoid the pore collapse during drying.

These studies provide a novel approach to synthesis of porous crosslinked networks in beads shape, starting from an unsaturated copolyimide. The experiments have shown that the discussed systems in which one of the reaction partners is a polymer, respect the principles of the suspension polymerization, supporting the obtained results. The proposed approach opens new perspectives for obtaining high performance complex systems, expected to exhibit potential functional advantages for surface-related applications.

Table 6 Kinetic parameters of the main thermal decomposition stage

Samples	n	Ea (kJ/mol)	lnA
CPI	1.26±0.002	162.26±3.38	21.67±0.58
BMI	0.24±0.002	222.90±3.76	30.41±0.63
1.I	2.16±0.003	270.49±4.06	40.64±0.70
4.I	3.02±0.002	374.07±3.58	59.15±0.62
11. III	1.88±0.004	211.44±5.07	30.61±0.88
14. III	2.49±0.001	346.64±1.66	53.99±0.29

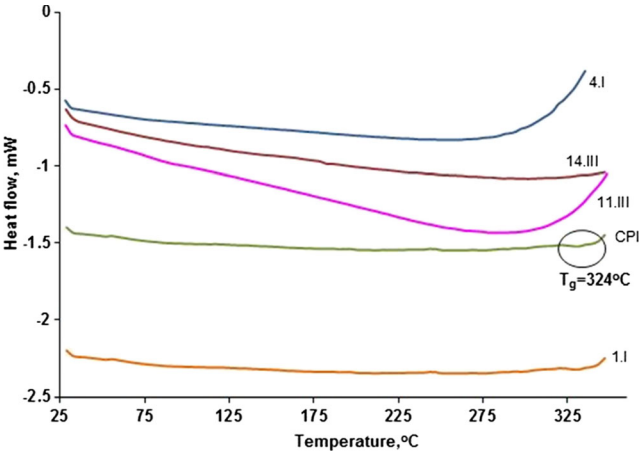

Fig. 10 DSC curves read after the second heating at a rate of 10°C from 25 to 350°C

Acknowledgments This work is financially supported from PN-II-ID-PCE-2011-3-0937 Project No. 302/5.10.2011.

References

1. Dusek K (1982) Network formation by chain crosslinking (co)polymerization, in Developments in polymerization-3. In: Haward RN (ed) ScD. Publ. Appl. Science publisher in LTD, England
2. Okay O (2000) Macroporous copolymer networks. Prog Polym Sci 25(6):711–779
3. Clarisse M, Queirys Y, Barbosa C, Barbosa L, Lucas E (2012) Synthesis and Characterization of Polymeric Resins Based on Methyl Methacrylate and Divinylbenzene. Chemistry & Chemical Technology, The Journal 6(2):145–152
4. Gawdzik B, Sobiesiak M (2003) Chemical composition of plasma treated polyimide microspheres. Appl Surf Sci 214:52–55
5. Gao JG, Zhang Y, Yu YF, Han YC, Zhang BZ, Gao CH (2011) Preparation of chitosan microspheres loading of 3,5-dihydroxy-4-i-propylstilbene and in vitro release. J Polym Res 18:1501–1508
6. Kun KA, Kunin R (1968) Macroreticular resins. III. Formation of macroreticular styrene–divinylbenzene copolymers. J Polym Sci Part A-1:Polym Chem 6:2689–2701
7. Sederel WL, De Jong GJ (1973) Styrene–divinylbenzene copolymers. Construction of porosity in styrene divinylbenzene matrices. J App Polym Sci 17(9):2835–2846
8. Brooks BW (1990) Basis aspects and recent developement in suspension polymerisation. Makromol Chem, Macromol Symp 35/36:121–140
9. Svec F, Frechet MJ (1996) New design of macroporous polymers and supports from separation to biocatalysis. Science 273:205–21
10. Bortel E (1965) Porous ion exchangers. I. Porosity of styrene-divinylbenzene copolymers. Przemysl Chem 44:255–270
11. Nicolescu T-V, Meouche W, Branger C, Margaillan A, Sarbu A, Donescu D (2012) Tailor-made polymer beads for gallic acid recognition and separation. J Polym Res 19:2–13
12. Flory PJ (1953) Principles of Polymer Chemistry. Press, Cornell University
13. Chen CW, Chen CY, Lin CL (2011) Preparation of monodisperse poly (methyl methacrylate)microspheres: effect of reaction parameters on particle formation, and optical performances of its diffusive agent application. J Polym Res 18:587–594
14. Grochowicz M, Bartnicki A, Gawdzik B (2008) Preparation and Characterization of Porous Polymeric Microspheres Obtained from Multifunctional Methacrylate Monomers. J Polym Sci: Part A: Polym Chem 46(18):6165–6174
15. Sroog CE (1991) Polyimides. Prog Polym Sci 16(4):561–694
16. Mathews AS, Kim I, Ha CS (2007) Synthesis, characterization, and properties of fully aliphatic polyimides and their derivatives for microelectronics and optoelectronics applications. Macromol Res 15(2):114–128
17. Wilson D, Stenzenberger HD, Hergenrother PM (1990) Polyimides. Chapman and Hall, New York
18. Chisca S, Musteata VE, Stoica I, Sava I, Bruma M (2013) Effect of the chemical structure of aromatic-cycloaliphatic copolyimide films on their surface morphology, relaxation behavior and dielectric properties. J Polym Res 20:111–121
19. Ree M (2006) High performance polyimides for applications in microelectronics and flat panel displays. Macromol Res 14(1):1–33
20. Ando S (2004) Optical Properties of Fluorinated Polyimides and Their Applications to Optical Components and Waveguide Circuits. J Photopolym Sci Technol 17(2):219–232
21. Cosutchi AI, Hulubei C, Stoica I, Ioan S (2011) A new approach for patterning epiclon-based polyimide precursor films using a lyotropic liquid crystal template. J Polym Res 18(6):2389–2402
22. Mittal KL (1984) Polyimides: synthesis, characterization and applications, vol 1 & 2. Springer (Plenum Press), New York
23. Ismail AF, Aziz F (2012) Chemical Cross-Linking Modifications of Polymeric Membranes for Gas Separation Applications, Chap. 11. In: Hilal N, Khayet M, Wright CJ (eds) Membrane Modification Technology and Applications. CRC Press, US
24. Takekoshi T (1996) In: Ghosh MK, Mittal KL (eds) Polyimides: Fundamentals and Applications, vol 1, 1st edn. Marcel Dekker, New York
25. Chen JC, Tseng WY, Tseng IH, Tsai MH (2011) High transparency and thermal stability of alicyclic polyimide with crosslinking structure by triallylamine. Adv Mater Res 287–290:1388–1396
26. Ioan S, Hulubei C, Popovici D, Musteata VE (2013) Origin of dielectric response and conductivity of some alicyclic polyimides. Polym Eng Sci 53(7):1430–1447
27. Kumar SV, Yu HC, Choi J, Kudo K, Jang YH, Chung CM (2011) Structure–property relationships for partially aliphatic polyimides. J Polym Res 18:1111–1117
28. Chen G, Pei X, Liu J, Fang X (2013) Synthesis and properties of transparent polyimides derived from trans- and cis-1,4-bis(3,4-dicarboxyphenoxy)cyclohexane Dianhydrides. J Polym Res 20: 159–169
29. Hou Y, Chen G, Pei X, Fang X (2012) Synthesis and characterization of novel optically transparent and organosoluble polyimides based on diamines containing cyclohexane moiety. J Polym Res 19:9955–9963
30. Barzic AI, Stoica I, Fifere N, Vlad CD, Hulubei C (2013) Morphological effects on transparency and absorption edges of some semi-alicyclic polyimides. J Polym Res 20:130–137
31. Brock T, Sherrington DC, Swindell J (1994) Synthesis and characterisation of porous particulate polyimides. J Mater Chem 4(2):229–236
32. Sherrington D (1998) Preparation, structure and morphology of polymer supports. Chem Commun 21:2275–2286
33. Fu GD, Li GL, Neoh KG, Kang ET (2011) Hollow polymeric nanostructures—Synthesis, morphology and function. Prog Polym Sci 36(1):127–167
34. Ishizaka T, Kasai H (2012) In: Abadie MJM (ed) High Performance Polymers - Polyimides Based - From Chemistry to Applications, Fabrication of Polyimide Porous Nanostructures for Low-k Materials. Novi Sad, InTech
35. Hren J, Polanc S, Kočevar M (2008) The synthesis and transformations of fused bicyclo[2.2.2]octenes. Special Issue Reviews and Accounts ARKIVOC 209–231 ISSN 1551–7012
36. Ioan S, Cosutchi AI, Hulubei C, Macocinschi D, Ioanid G (2007) Surface and interfacial properties of poly(amic acid)s and polyimides. Polym Eng Sci 47(4):381–389
37. Dix LR, Ebdon JR, Flint NJ, Hodge P, O'Dell R (1995) Chain extension and crosslinking of telechelic oligomers—I. Michael additions of bisamines to bismaleimides and bis(acetylene ketone)s. Eur Polym J 31(7):647–652
38. Freeman ES, Carroll B (1958) The Application of Thermoanalytical Techniques to Reaction Kinetics: The Thermogravimetric Evaluation of the Kinetics of the Decomposition of Calcium Oxalate Monohydrate. J Phys Chem 62(4):394–397
39. Brunauer S (1957) Adsorption of Gases and Vapors Princeton University Press. New Jersey Press, New York

40. Choi YS, Hong SR, Lee YM, Song KW, Park MH, Nam YS (1999) Study on gelatin-containing artificial skin: I. Preparation and characteristics of novel gelatin-alginate sponge Biomaterials 20(5):409–417
41. Park HY, Song IH, Kim JH, Kim WS (1998) Preparation of thermally denatured albumin gel and its pH-sensitive swelling. Int J Pharm 175(2):231–236
42. ISO 25178–2:2012, Geometrical product specifications (GPS) - Surface texture: Areal - Part 2: Terms, definitions and surface texture parameters
43. Nic M, Jirat J, Kosata B updates compiled by Jenkins A (1997) IUPAC. Compendium of Chemical Terminology, 2nd ed. (the "Gold Book"). Compiled by A. D. McNaught and A. Wilkinson. Blackwell Scientific Publications, Oxford. XML on-line corrected version: http://goldbook.iupac.org
44. Ishida H, Wellinghoff ST, Baer E, Koenig JL (1980) Spectroscopic Studies of Poly [N, N'-bis(phenoxyphenyl)pyromellitimide]. 1. Structures of the Polyimide and Three Model Compounds. Macromolecules 13(4):826–834
45. Kotoulas C, Kiparissides C (2006) A generalized population balance model for the prediction of particle size distribution in suspension polymerization reactors. Chem Eng Sci 61(2):332–346
46. Chatzi EG, Kiparissides C (1994) Drop size distributions in high holdup fraction dispersion systems: effect of the degree of hydrolysis of PVA stabilizer. Chem Eng Sci 49(24, Part 2):5039–5052
47. Jalili K, Abbasi F, Nasiri M, Ghasemi M, Haddadi NDE (2009) Preparation and Characterization of Expandable St/MMA Copolymers Produced by Suspension Polymerization. J Cell Plast 45:197–224
48. Ioan S, Filimon A, Hulubei C, Stoica I, Dunca S (2013) Origin of rheological behavior and surface/interfacial properties of some semi-alicyclic polyimides for biomedical applications. Polym Bull 70(10): 2873–2893
49. Jahanzad F, Sajjadi S, Brooks BW (2005) Comparative Study of Particle Size in Suspension Polymerization and Corresponding Monomer−Water Dispersion. Ind Eng Chem Res 44(11):4112–4119
50. Svec F, Frechet JMJ (1995) Temperature, a Simple and Efficient Tool for the Control of Pore Size Distribution in Macroporous Polymers. Macromolecules 28(22):7580–7582
51. Koenhen DM, Smolders CA (1975) The determination of solubility parameters of solvents and polymers by means of correlations with other physical quantities. J Appl Polym Sci 19(4):1163–1179
52. van Krevelen DW, te Nijenhuis K (2009) Properties of Polymers: Their Correlation with Chemical Structure; their Numerical Estimation and Prediction from Additive Group Contributions. Elsevier Science, Amsterdam
53. Allan F, Barton M (1983) Handbook of Solubility Parameters, Ph.D. Thesis. CRC Press, 153–157
54. Chompff A J, Newman S, Society A C (1971) Polymer networks: structure and mechanical properties: proceedings. Press, Plenum
55. Small PA (1953) Some factors affecting the solubility of polymers. J Appl Chem 3(2):71–80
56. Stoica I, Barzic AI, Hulubei C, Timpu T (2013) Statistical Analysis on Morphology Development of Some Semi-alicyclic Polyimides Using Atomic Force Microscopy Microsc. Res Techn 76:503–513
57. Marcu Puscas T, Signorini M, Molinari A, Straffelini G (2003) Image analysis investigation of the effect of the process variables on the porosity of sintered chromium steels. Mater Character 50(1):1–10
58. Dickie RA, Labana SS, Bauer RS, Science ACSDoPM, Engineering (1988) Cross-Linked Polymers: Chemistry, Properties, and Applications. American Chemical Society
59. Silverstein MS, Cameron NR, Hillmyer MA (2011) Porous Polymers. Wiley
60. Calvino-Casilda V, Lopez-Peinado AJ, Vaganova E, Yitzchaik S, Pacios IE, Pierola IF (2008) Porosity Inherent to Chemically Crosslinked Polymers. Poly(N-vinylimidazole) Hydrogels. J Phys Chem B 112(10):2809–2817
61. Poinescu I, Vlad C, Carpov A, Ioanid A (1988) On the structure of macroreticular styrene-divinylbenzene copolymers. Die Angewandte Makromolekulare Chemie 156(1):105–121